

## The dependence of the energy density states on the substitution of chemical elements in the $\text{Se}_6\text{Te}_{4-x}\text{Sb}_x$ thin film

B. A. Ahmed<sup>a</sup>, J. S. Mohammed<sup>b</sup>, R. N. Fadhil<sup>a</sup>, K. A. Jasim<sup>a</sup>, A. H. Shaban<sup>c\*</sup>,  
A. H. Al Dulaimi<sup>b</sup>

<sup>a</sup>Department of physics, College of Education for pure Sciences Ibn AlHaitham,  
University of Baghdad, Baghdad, Iraq

<sup>b</sup>Department of Physics, College of Science, University of Diyala, Iraq

<sup>c</sup>College of Science, University of Baghdad, Baghdad, Iraq

The energy density state are the powerful factor for evaluate the validity of a material in any application. This research focused on examining the electrical properties of the  $\text{Se}_6\text{Te}_{4-x}\text{Sb}_x$  glass semiconductor with  $x=1, 2$  and  $3$ , using the thermal evaporation technique. D.C electrical conductivity was used by determine the current, voltage and temperatures, where the electrical conductivity was studied as a function of temperature and the mechanical electrical conduction were determined in the different conduction regions (the extended and localized area and at the Fermi level). In addition, the density of the energy states in these regions is calculated using the mathematical equations. The constants of energy density states are determined, namely the electron hopping distance, the width of the tails, and pre - exponential factor. The densities of the energetic states (extended  $N(E_{\text{ext}})$ , localize  $N(E_{\text{loc}})$  and at the Fermi states  $N(E_f)$  will be calculated in each of the regions. Moreover, the effect of partial substitution of Se with antimony on energy states and degree of randomness, results observed that the energy densities changing with an increase antimony Sb concentration.

(Received January 14, 2022; Accepted April 29, 2022)

*Keywords:* Glass semiconductor, Amorphous silicon, Chalcogenides

### 1. Introduction

The amorphous semiconductors have an optical properties with special ranges in transmittance at infrared region and have a high refractive index (2-4). The optical band gap is suitable for altered applications and devices. The chalcogenides thin films were developed in photovoltaic coating.

In recent years, photovoltaic coatings for chalcogenides (thin film) have been produced for sensing, visualization, solar radiation absorption, verification, photo thermal equipment, and display. [1]The optical characteristics are very important in applications of optoelectronics devices. These properties are absorption coefficient, refractive indices, and optical band gap. [2] [3]Due to their possible uses in the field of optics, silicon-rich chalcogenides are the most studied and assimilated semiconductors. [4] [5]The lower sensitivity and the shorter life span in these materials will reduce the ability of using these materials in applications which can be reduced through mixing Se with activators like Te, Sb, Bi, Ge, As, Cu etc. [6] [7]. This process will enhance the electric characteristics (sensitivity, conductivity, thermal stability and aging effects) [8]. The result of replacing Sb into the Se-Te base matrix, is  $\text{Se}_6\text{Te}_{4-x}\text{Sb}_x$  chalcogenide system with different ( $x=1, 2$  and  $3$ ).

---

\* Corresponding authors: [auday.h@sc.uobaghdad.edu.iq](mailto:auday.h@sc.uobaghdad.edu.iq)  
<https://doi.org/10.15251/CL.2022.194.301>

## 2. The theory part

Semiconductor materials have a relatively small energy gap between the conduction band and the valence band with a value close to the thermal energy (KT), and when the temperature of the semiconductor increases it will lead to an increase in the concentration of electrons in the conduction band if the material is of the negative type (n type), or It may increase the concentration of holes in the valence tape if the material is of the positive (p-type) type. By increasing the temperature to room temperature, the atoms of the impurities are ionized according to the type of impurity (the energy of the impurities). If we raise the temperature more than that, then you will get an increase in both the electrons and the holes caused by the excited electrons from the valence band to the conduction band, and this is known as electron hole generation.

The electrical conductivity changes with the temperature of the semiconductor as shown in the relationship:

$$\sigma = \sigma_0 e^{\left(-\frac{\Delta E}{kT}\right)} \quad (1)$$

where  $\sigma_0$  and  $\Delta E$ : represented to pre expansion factor and activation energy (eV), carriers are excited about protracted states to showcase activation Energy  $E_C - E_F$  (or  $E_F - E_V$ ).  $T$ : temperature (k).  $k$  is the Boltzmann constant.

The contribution of electrical conductivity is predominantly dependent on the different temperature ranges to which the semiconductors are exposed, especially in the chalcogenide glass semiconductor, over the temperature ranges. At lower temperatures, the conductivity can be by electron or hole jumping between the local energy states located near the Fermi level. But at medium temperatures, the electrical conductivity is according to the levels of the local energy states at the tails of the energy band, where the electronic charges are transferred by jumps between the local levels in the region of the tails of the energy bands. As for high temperatures, the electrical conductivity is between levels of extended energy states of the conduction and valence beams.

Therefore, equation 1 includes in most cases three terms, each of these terms represents a conduction mechanism for a region of the above regions, where equation 1 becomes as follows [9]:

$$\sigma = \sigma_{01} e^{\left(-\frac{E_1}{kT}\right)} + \sigma_{02} e^{\left(-\frac{E_2}{kT}\right)} + \sigma_{03} e^{\left(-\frac{E_3}{kT}\right)} \quad (2)$$

Through equation 2, the relationship between electrical conductivity and the different temperature ranges to which a semiconductor is exposed can be depicted. As for the first term, it represents the electrical conductivity of high temperatures, it is possible to calculate the intensity of the extended energy states in the two bundles of conduction and valence and the following equation [10]

$$\sigma_{0ext.} = \left(\frac{1}{6}\right) e^2 a^2 V_e N(E_C) \quad (3)$$

where electron frequency  $V_e = \frac{\hbar}{a^2 M}$  and Interatomic distance  $a = 0.026 \frac{e^2}{h\sigma_0}$  therefor  $N(E_{ext})$  [9]:

$$\square N(E_{ext}) = \left[\frac{6m}{e^2 \hbar}\right] \sigma_{0ext} \quad (4)$$

As for the second term of the equation 2, it represents the conductivity at medium temperatures, from which it computes the activation energy and the factor that precedes the exponent and then calculates the density of local energy states in the region of the tails of the energy bands. According to the following equation:

$$\square N(E_{loc}) = \left[\frac{6}{e^2 V_{ph} R^2}\right] \sigma_{02} \quad (5)$$

where the phonon's frequency indicated by  $V_{ph}$ , distance  $R$  hopping between two localize states.

At lower temperatures it is possible to extract the activation energy  $E_3$  and the pre-exponential factor  $\sigma_{03}$  the exponent from the third term of equation 2, and then calculate the density of local energy states near the Fermi level. According to the following equation [11]:

$$\sigma_{03} = \left(\frac{1}{6}\right) e^2 V_{ph} R^2 N(E_F) \quad (6)$$

where  $N(E_F)$  is the state density near the Fermi level, and  $e$  is the electron charge.

$$\text{So, } R = 0.7736 \left[ \frac{\Delta E a^{-1}}{N(E_C)(kT)^2} \right]^{0.25}$$

$$\Delta E = E_1 - E_2$$

$\alpha^{-1} = 10^{-7} \text{cm}$  (optical absorption coefficient) while  $N(E_C)$  represent the density of extended state.

### 3. Experimental

The chalcogenide  $\text{Se}_6\text{Te}_{4-x}\text{Sb}_x$  glass semiconductor with  $x=1, 2$  and  $3$ , (A, B, C), were prepared using thermal evaporation technique. After being pre-cleaned, a sufficient volume of starting materials such as selenium, tellurium, and antimony was weighed and moved to quartz ampoules. The ampoules containing these starting materials were then emptied and sealed with oxy-acetylene flame burners at a pressure of  $10^{-4}$  tor. After that, the ampoules were steadily heated in an electric furnace to  $800 \text{ K}$  at a rate of  $50 \text{ K / hour}$ , after which the ampoules were maintained at this temperature  $12$  hours. The materials ( $\text{Se}_6\text{Te}_{4-x}\text{Sb}_x$  with a purity of  $99.99\%$ ) were evaporated in a molybdenum boat. Thermal evaporation was performed in the system at a base pressure of  $9 \times 10^{-5} \text{ Pa}$ , and the distance between the substrate holder and the molybdenum boat was  $30 \text{ cm}$ . The thickness of the films was measured using a lateral surface gauge, and the thickness of the samples was found to range between  $80-90 \text{ nm}$ . The electrical conductivity of the membranes was measured in the temperature range of  $303-423 \text{ K}$  by placing the samples in an electric furnace, measuring the current and the filtration passing through the sample with changing and raising the temperature of the furnace, and then calculating the electrical conductivity with respect to temperature. The adoption of the configuration of the obtained electrical parameters helps us to understand the effect of  $\text{Sb}$  on the energy density of states for  $\text{Se}_6\text{Te}_{4-x}\text{Sb}_x$  glass semiconductor.

### 4. Results and discussion

Continuous electrical measurements (voltage and current) were investigated at low, medium and high temperatures of the three samples with partial substitution of tellurium  $\text{Te}$  with the antimony  $\text{Sb}$  as shown in figure 1.

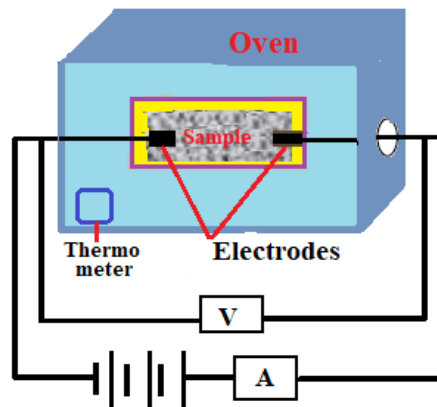


Fig. 1. Practical circuit.

The electrical conductivity of all thin-alloy films for different temperatures was calculated. The relationship between electrical conductivity and temperature is drawn in the figure 2. Through this figure, it is noticed that the conductivity of all samples has temperature dependence and the behavior of semiconductors. The electrical conductivity increased with increasing temperature, indicating the semiconductor behavior of all alloys. Moreover, electrical conductivity increases with increasing Sb content. The conductivity data were analyzed to characterize the possible mechanisms in the thin films, especially the process that is thermally activated. The contrast is shown between  $\ln \sigma$  versus  $1000/T$  for three typical  $\text{Se}_6\text{Te}_{4-x}\text{Sb}_x$  glass semiconductor films. The three curves indicate that conduction through thermal activation have three different mechanisms. It is also noted that each curve consists of three different parts from which three different activation energies the pre-exponential factors were obtained, according to the equation (1), representing the conduction mechanisms for all levels regions.

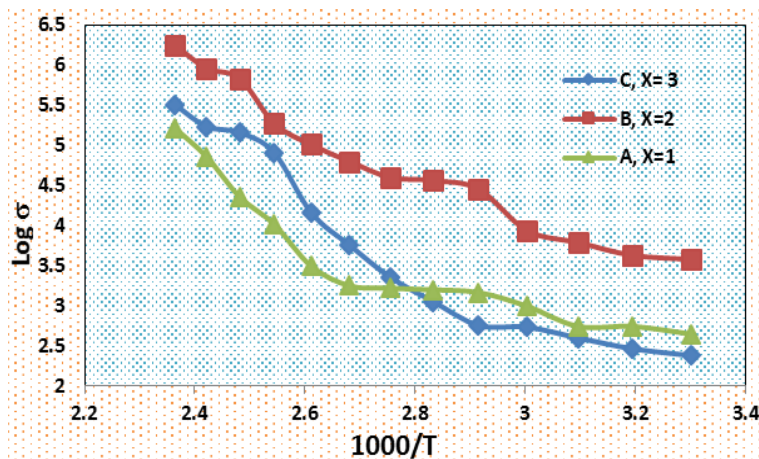


Fig. 2. The conductivity vs temperatures, for  $\text{Se}_6\text{Te}_{4-x}\text{Sb}_x$  glass semiconductor with  $x=1, 2$  and  $3$ .

With the help of computer programs, the activation energies  $\Delta E_1$ ,  $\Delta E_2$  and  $\Delta E_3$  and the pre-exponential factor  $\sigma_{01}$ ,  $\sigma_{02}$  and  $\sigma_{03}$  were calculated for each of these parts, respectively. They are listed in Table 1. The relationship between activation energies  $\Delta E_1$ ,  $\Delta E_2$  and  $\Delta E_3$  and Sb concentration was drawn in the figure 3. Through this figure, it is noticed that the  $\Delta E_1$ ,  $\Delta E_2$  and  $\Delta E_3$  of all samples increase with increasing Sb concentration, these results are in agreement with those of the researchers in reference [12] [13]

Table 1. The value of activation energies  $\Delta E_1$ ,  $\Delta E_2$  and  $\Delta E_3$  and the pre-exponential factor  $\sigma_{01}$ ,  $\sigma_{02}$  and  $\sigma_{03}$  for  $Se_6Te_{4-x}Sb_x$  glass semiconductor with  $x=1, 2$  and  $3$ .

X	$\Delta E_1$ (ev)	$\Delta E_2$ (ev)	$\Delta E_3$ (ev)	$\sigma_{01}$ ( $\Omega^{-1} \cdot \text{cm}^{-1}$ )	$\sigma_{02}$ ( $\Omega^{-1} \cdot \text{cm}^{-1}$ )	$\sigma_{03}$ ( $\Omega^{-1} \cdot \text{cm}^{-1}$ )
1	0.191	0.233	0.186	$1.73 \times 10^2$	90	2.37
2	0.805	0.299	0.349	$1.43 \times 10^3$	$1.67 \times 10^3$	71.05
3	0.848	1.02	0.845	$8.94 \times 10^3$	$3.38 \times 10^4$	$4.3 \times 10^2$

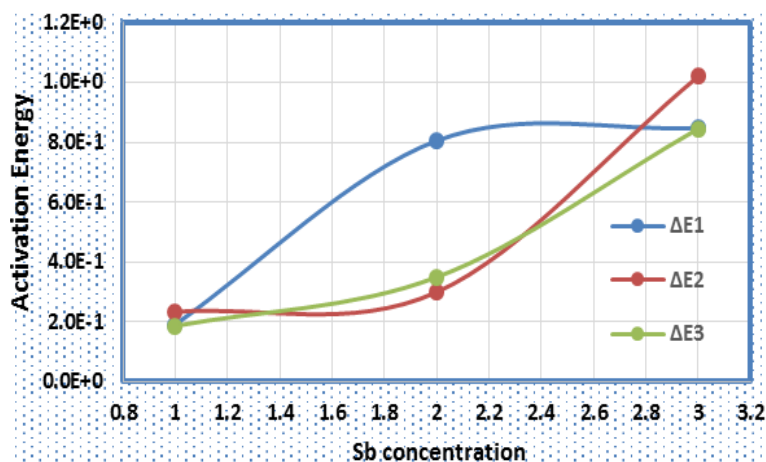


Fig. 3. Activation energies  $\Delta E_1$ ,  $\Delta E_2$  and  $\Delta E_3$  with respect to the concentration of Sb for the glass semiconductor  $Se_6Te_{4-x}Sb_x$ .

Figure 4 shows the hopping distance ( $R$ ) and  $\Delta E$ : width of energy tail and interatomic distance  $a$  computed from the equations in the theoretical parts as a function of the concentration of the antimony element, where in general it is noticed that there is a decrease in both  $R$  and  $\Delta E$  and  $a$  with increasing the concentration of the antimony component, and this indicates that there is condensation in the energy levels of the bands, therefore these parameters decreased [14]. In addition, the decrease in the local states leads to the tendency of the compound to the crystalline state, moving away from randomness, and these results are consistent with the results obtained in reference [14]. The data shown in table 2.

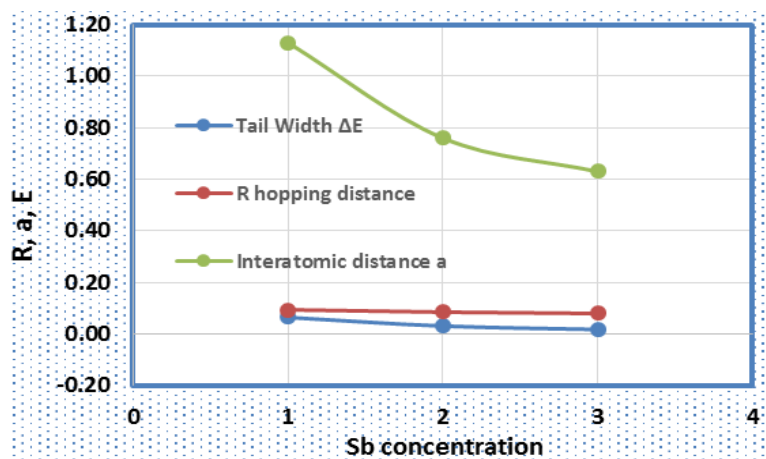


Fig. 4.  $R$ : hopping distance between two localized states, width of energy tail  $\Delta E$ : and interatomic distance  $a$  as a function of the concentration of the antimony element.

Through Table 1 and the application of the equations of the theoretical part, the densities of the energetic states  $N(E_{ext})$ ,  $N(E_{loc})$  and  $N(E_F)$  will be calculated in each of the three regions (extended, localized and at the Fermi level, respectively) according to equations 4, 5 and 6. In addition to calculating the width of each tail width band from the different between activation energies  $\Delta E_1$  and  $\Delta E_2$ . We discuss these accounts in detail as follows:

In the first zone, the conduction zone at higher temperatures, the predominant mechanism is the conduction across the extended states. It is expressed in the first part of equation (1), in which the activation energy in the extended states  $E1 = (EC - EF)$  or  $EF - EV$  [15]

Calculating the density of energy states in an extended region are listed in Table 1. The results are illustrated in Table 2. Antimony concentration will affects the density of extended energy states Figure 5 represents for three samples. Curve (a) represents the relationship of the density of extended energy states with respect to the antimony concentration.

Table 2. The properties of  $Se_6Te_{4-x}Sb_x$  glass semiconductor with respect to Sb concentration.

x	Tail Width $\Delta E$ (ev)	R(A <sup>0</sup> )	a (A <sup>0</sup> )	$N(E_{ext}) \times 10^{18}$ (ev <sup>-1</sup> cm <sup>-3</sup> )	$N(E_{loc}) \times 10^{16}$ (ev <sup>-1</sup> cm <sup>-3</sup> )	$N(E_F) 10^{13}$ (ev <sup>-1</sup> cm <sup>-3</sup> )
1	0.642	0.936	1.13	1.826	1.464	12.5
2	0.306	0.847	0.76	1.548	167	5.72
3	0.172	0.792	0.63	18.37	554	3.197

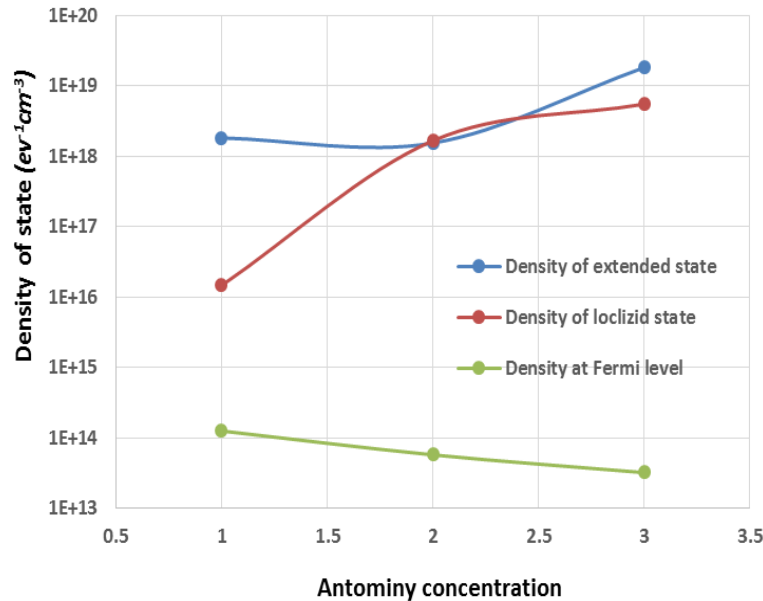


Fig. 5. The densities of energy states with respect to Sb concentration for  $Se_6Te_{4-x}Sb_x$  glass semiconductor.

While the curve b expresses the density of the local states at the tails of the band, where it was noticed that there is a decrease in the density when increasing from  $(1.464 \text{ to } 167) \times 10^{16}$  (ev<sup>-1</sup>cm<sup>-3</sup>) by increase antimony to 2 and then increasing to  $554 \times 10^{16}$  (ev<sup>-1</sup>cm<sup>-3</sup>) with  $x = 3$

As for the curve, it expresses the density of local states at the Fermi level, where it was noticed that there is an increase in the density of energy states from  $(12.5 \text{ to } 3.197) \times 10^{13}$  (ev<sup>-1</sup>cm<sup>-3</sup>) with an increase in the antimony.

Figure 5 shows the densities of states for three regions (extended and localized in the tails of the beams and at the Fermi level) calculated from eq. 3, 6 and 9 as a function of the concentration of the antimony element, as it is generally noticed that both the densities of the extended and localized energy states in the tails of the beams increase with the increase in the concentration of the antimony element, while The densities of the local energy states at the Fermi

level decrease with the increase in the concentration of the antimony element, and this indicates that the randomness in the crystal structure of the compound decreases with the increase in the concentration of the antimony element, meaning that the crystallization increased with the increase in the concentration of the antimony element and this is the reason for improving the continuous electrical conductivity in addition to the increase in the stability of the compound [16]- [17] and these results Corresponds to the results obtained by the two papers in reference [18].

## 5. Conclusion

The  $\text{Se}_6\text{Te}_{4-x}\text{Sb}_x$  glass semiconductor with  $x=1, 2$  and  $3$  was prepared by the solid-state reaction method. Thin films of  $\text{Se}_6\text{Te}_{4-x}\text{Sb}_x$  glass were then deposited onto clean glass substrates using a vacuum evaporation technique. Electrical conductivity was measured with respect to temperature. The electrical conductivity for all samples changed with increasing the concentration of the antimony element. The results shows that the temperature generate a three conduction mechanisms. Moreover, the change in the electrical conduction behavior of the  $\text{Se}_6\text{Te}_{4-x}\text{Sb}_x$  glass samples was due to the cultivation of trapping states for the level of antimony structure. The conduction activation energies and jump distances were calculated with respect to temperature in the three low, high and medium temperature regions. The densities of the extended and local states were calculated at the tails states and the Fermi level, where it was found that all of them increase with the increase antimony concentration and that the densities of the energy states in the extended region is much greater than the localized regions.

## References

- [1] A. Hmood, A. Kadhim, H. Abu Hassan . (2012). Superlattices and Microstructures, 825-833; <https://doi.org/10.1016/j.spmi.2012.04.001>
- [2] Abbas K.Saadon, Mustafa Mohammed Ali, Kareem A.Jasim & Duraid H.Younis . (2014). Study the Physical and Dielectric Properties of Ferrite - Sic Composite, i . . Ibn Al-Haitham Jour. for Pure & Appl. Sc, 91-96.
- [3] Kareem A. Jasim, Rihab Nassr Fadhil, Auday H. Shaban, Harith I. Jaafar, Bushra K.H. Maiyaly, Suad H. Aleabi, Ebtisam M-T. Salman . (2019). PIE, Progress in Indus, 163-172; <https://doi.org/10.1504/PIE.2019.099357>
- [4] Abdulateef, A. N., Alsudani, A., Chillab, R. K., Jasim, K. A., & Shaban, A. H. . ( 2020 ). Calculating the Mechanisms of Electrical Conductivity and Energy Density of States for  $\text{Se}_{85}\text{Te}_{10}\text{Sn}_5\text{-xIn}_x$  Glasses Materials. Journal of Green Engineering,, 5487-5503.
- [5] Adak, M. K., Das, A., & Debasis, D. ( 2020 ). Materials in Electronics, 6786-6795; <https://doi.org/10.1007/s10854-020-03237-6>
- [6] Alvi, M. A. (2013). Nanoscale Research Letters, 1-10; <https://doi.org/10.1186/1556-276X-8-148>
- [7] Frumar, M. &. (1987). Journal of Non-Crystalline Solids , 1139-1146; [https://doi.org/10.1016/0022-3093\(87\)90273-0](https://doi.org/10.1016/0022-3093(87)90273-0)
- [8] Haider, H. M. (2019). AIP Conf. Proc, 1-7; <https://doi.org/10.1063/1.5116960>
- [9] Hassanien, A. S., & Akl, A. A. . (2016). Superlattices and Microstructures, 153-169; <https://doi.org/10.1016/j.spmi.2015.10.044>
- [10] Jasim, K. A., Fadhil, R. N., Shaban, A. H., Jaafar, H. I., Maiyaly, B. K., Aleabi, S. H., & Salman, E. M. . (2019). PIE Progress in Industrial Ecology, an Internat, 163-172; <https://doi.org/10.1504/PIE.2019.099357>
- [11] Kadhim, B. B., Risan, R. H., Shaban, A. H., & Jasim, K. A. (2019) . AIP Conference Proceedings , 020062- 5; <https://doi.org/10.1063/1.5116989>
- [12] Khan, B. A. (1984). Journal of non-crystalline solids, 35-42; [https://doi.org/10.1016/0022-3093\(84\)90204-7](https://doi.org/10.1016/0022-3093(84)90204-7)

- [13] Mott, N. F., & Davis, E. A. . (2012). *Electronic processes in non-crystalline materials*. Oxford university press., 591.
- [14] Ram, I. S., Kumar, S., Singh, R. K., Singh, P., & Singh, K. . (2015). *AIP Advances*, 1-7; <https://doi.org/10.1063/1.4929577>
- [15] Tohge, N., Matsuo, H., & Minami, T. . (1987). *Journal of Non-Crystalline Solids*, 809-816; [https://doi.org/10.1016/S0022-3093\(87\)80685-3](https://doi.org/10.1016/S0022-3093(87)80685-3)
- [16] Troles, J., & Brilland, L. . (2014). Chalcogenide microstructured optical fibers for infrared applications. In *Chalcogenide glasses*. Woodhead Publishing, 411-437; <https://doi.org/10.1533/9780857093561.2.411>
- [17] Vanitha, M. K., Rao, M. H., Asokan, S., & Ramesh, K. . (2013). *Journal of Physics and Chemistry of Solids*, 804-810; <https://doi.org/10.1016/j.jpics.2013.01.010>
- [18] Yinzhu, J. Y. ( 2012). Abnormal behavior in electrical transport properties of cobalt doped tin oxide thin films. *Journal of Materials Chemistry*, 213-218.